



Disinfection mechanism of *E. coli* by CNT-TiO₂ composites: Photocatalytic inactivation vs. physical separation

Yuta Shimizu^a, Mohamed Ateia^{b,*}, Manna Wang^a, Dion Awfa^a, Chihiro Yoshimura^a

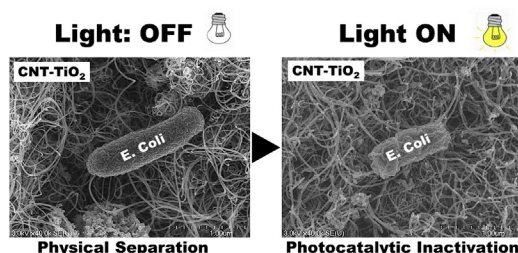
^a Department of Civil and Environmental Engineering, School of Environment and Society, Tokyo Institute of Technology, 2-12-1, M1-4, Ookayama, Meguro-ku, Tokyo, 152-8552, Japan

^b Department of Environmental Engineering and Earth Science, Clemson University, SC, 29634, USA

HIGHLIGHTS

- CNT and its composites with TiO₂ had much higher disinfection efficiencies than bare TiO₂.
- The physical bacterial capture was the dominant disinfection mechanism.
- The highest disinfection rate was found at an optimum CNT:TiO₂ ratio of 5:1.
- •OH was the influencing reactive oxygen species on the photocatalytic disinfection.

GRAPHICAL ABSTRACT



ARTICLE INFO

Article history:

Received 19 April 2019

Received in revised form

26 June 2019

Accepted 1 July 2019

Available online 4 July 2019

Handling Editor: Xiangru Zhang

Keywords:

Magnetic carbon nanotube

Titanium dioxide

Photocatalysis

Disinfection

E. coli

ABSTRACT

Magnetic carbon nanotube (MCNT) composites with titanium dioxide (TiO₂) have an enhanced photocatalytic disinfection efficiency (i.e. higher disinfection rate) and better applicability (i.e. solar light applicability and catalyst separation using its magnetic property) than bare TiO₂ and/or MCNT. However, the role and mechanism of MCNT in the disinfection process are still unclear. Therefore, this study aimed at investigating the disinfection mechanism of *Escherichia coli* using MCNT-TiO₂ nanocomposites under various conditions (i.e. the presence and absence of light and reactive oxygen species scavengers, and different MCNT-TiO₂ ratio) and photocatalytic disinfection models. The results showed that (i) MCNT and its nanocomposites with TiO₂ had much higher disinfection efficiencies than bare TiO₂, (ii) the physical bacterial capture was the dominant disinfection mechanism, (iii) the higher disinfection rate was found at an optimum MCNT:TiO₂ ratio of 5:1 under the tested experimental conditions, (iv) hydroxyl radical (•OH) was the influencing reactive oxygen species on the photocatalytic disinfection using MCNT-TiO₂, and (v) good correlation between experimental parameters (i.e. carbon contents, surface area and concentration of MCNT-TiO₂) and the contribution rate of physical and photocatalysis reactions. The finding from this study and the methods proposed herein are essential for understanding the photocatalytic disinfection processes using TiO₂ and its carbonaceous nanocomposites, which can promote the application of photocatalytic disinfection process.

© 2019 Elsevier Ltd. All rights reserved.

1. Introduction

The occurrence of pathogens (e.g. viruses, bacteria, protozoa and algae) in water sources possess a high risk of contracting

* Corresponding author.

E-mail address: mohamedateia1@gmail.com (M. Ateia).

waterborne diseases, which include cholera, typhoid, hepatitis A and E, and polio (Bennett, 2008). Besides, certain gut commensal and pathogenic strains of *Escherichia coli* and other proteobacteria produce genotoxins implicated in colorectal cancer pathogenesis (Wilson et al., 2019). Therefore, water disinfection is essential for removing these pathogens from water. Chemical disinfectants (e.g. chlorine, chloramine, and ozone) can cause oxidative damage on pathogen cells, but the low removal efficiency of highly resistant pathogens (King et al., 1988), the large consumption of toxic chemicals and the risk of forming carcinogenic disinfection byproducts (DBPs) (Nieuwenhuijsen et al., 2000; Ryan M. Brookman et al., 2011; Li et al., 2017a, 2017b; Ateia et al., 2019) limit their application. Ultraviolet irradiation can inactivate pathogens through direct damage on DNA structure without using any chemical (Song et al., 2016; Li et al., 2017a, 2017b), but the reactivation of microorganisms through repair mechanisms and the energy consumption are major disadvantages. Hence, it is still a major challenge to develop antimicrobial agents that can effectively and safely remove pathogens.

Heterogeneous photocatalysis by semiconductors and engineered nano-materials (ENMs) present new alternative disinfection techniques for the removal of pathogens from water with high reactivity and no formation of DBPs (Ayekoe et al., 2017; Li et al., 2008). Among semiconductor photocatalysts, TiO_2 is the most promising material because it is non-toxic, cheap, chemically and biologically inert, photostable and highly reactive (Friedmann et al., 2010). The main disinfection mechanism was reported as the photochemical oxidation of the intracellular coenzyme by extracellular reactive oxygen species (ROS) (i.e. hydroxyl radical ($\cdot\text{OH}$)) (Ouyang et al., 2016). In addition, carbon nanotubes (CNT) is another ENMs that showed antibacterial activities, however, the major disinfection mechanisms were via the physical capture of the bacteria from water, the isolation of the bacterial cell envelope, and the rupture of cell wall (Moon and Kim, 2010; Suárez-Iglesias et al., 2017; Thines et al., 2017). Thus, CNT- TiO_2 nanocomposite could combine both disinfection mechanisms and shown higher and faster disinfection activity than bare TiO_2 (Ganguly et al., 2018; Krishna et al., 2005).

As shown in Table S1, different observations and hypothesis were found in the literature on the disinfection performance and mechanism by CNT- TiO_2 nanocomposites. Krishna et al. (2005) investigated the disinfection of *Bacillus cereus* and *E. coli* using bare TiO_2 and CNT- TiO_2 nanocomposites under UV light irradiation. The inactivation of *B. cereus* using CNT- TiO_2 was twice faster than with bare TiO_2 , while the authors reported 'no disinfection' of *E. coli* using CNT- TiO_2 , thus hypothesizing that the morphology of *E. coli* caused steric effect and hindered the contact between photocatalyst and cell wall. However, a recent study by Koli et al. (2016b) has reported on an enhanced photocatalytic antibacterial activity for *E. coli* using CNT- TiO_2 nanocomposites due to the presence of CNT under visible light. On the other hand, Kang et al. (2007) reported that CNT exhibited strong antimicrobial activity against *E. coli* and concluded that cell membrane damage by the direct contact with CNT aggregates is the likely mechanism leading to bacterial cell death. Another study by Moon and Kim (2010) illustrated that magnetic CNT can adsorb on bacterial cells and physically remove them from the solution by applying a magnetic field. Similarly, Akasaka and Watari (2009) found that CNT captured *Streptococcus mutans* in water and made the colony-forming unit decrease. Basically, the combination of CNT and TiO_2 indicated higher disinfection removal relative to the bare TiO_2 itself. Despite this potential, the understanding on the major enhancement mechanism of CNT in CNT- TiO_2 photocatalytic disinfection is still fragmentary, indicating knowledge gap that hinders our understanding of the disinfection mechanism by CNT- TiO_2

nanocomposites (Awfa et al., 2018).

Here in, we considered all limitation in the literature and designed this systematic study to elucidate the disinfection mechanisms of *E. coli* using MCNT- TiO_2 nanocomposites. Inherent MCNT- TiO_2 was chosen in this study due to easy magnetic separation and the preparation of MCNT itself will not affecting the chemical composition of external nanotube walls (i.e. same properties with CNT) (Ateia et al., 2017). To this end, our specific objectives were to evaluate: 1) the effect of CNT: TiO_2 mass ratios in the nanocomposite on the disinfection activity, 2) the inactivation efficiency under different doses of CNT- TiO_2 nanocomposites, 3) the role of different ROS on the system performance, and 4) the role of each component in the nanocomposite (i.e. CNT and TiO_2) in the disinfection process.

2. Materials and methods

2.1. Materials

A commercial industrial grade of CNT (multi-wall, purity > 92%, length 10–30 μm) with Brunauer-Emmet-Teller (BET) surface area >150 $\text{m}^2 \text{g}^{-1}$ was purchased from Chengdu Alpha Nano Technology, China. Titanium (IV) oxide P25, anatase (particle size < 25 nm) with BET surface area 45–55 $\text{m}^2 \text{g}^{-1}$ were used as a precursor of TiO_2 and purchased from Sigma-Aldrich, Japan. Permanent magnet (Nd-Fe-B MAGNET) was provided by Magna Co., Japan. Ethanol, sodium oxalate and isopropanol were purchased from FUJIFILM Wako Pure Chemical Co., Japan. *E. coli* K12 strains (NBRC3301) were provided by NITE Biological Resource Center, Japan. Luria-Bertani (LB) nutrient medium (L3022) and LB agar medium (L2897) were also sourced from Sigma-Aldrich, Japan.

2.2. Synthesis of magnetic CNT (MCNT- TiO_2) nanocomposites

MCNT was prepared according to the method reported by Ateia et al. (2017). Briefly, 0.5 g of as-received CNT was dispersed in 100 mL of ethanol solution followed by sonication. Next, the magnetic fraction of CNT was separated by a permanent magnet, and the non- and/or low-magnetic fractions were discarded. This cycle was repeated 3 times. The same procedure was repeated by using ultrapure water as a solvent. Afterwards, the material was dried at 105 °C overnight and stored at room temperature until use. The produced MCNT was used for MCNT- TiO_2 synthesis (Ateia et al., 2017, 2018).

MCNT- TiO_2 nanocomposites were prepared based on the electrostatic attraction method reported by Tarigh et al. (2015) with some modifications. First, MCNT was dispersed in ethanol and sonicated for 60 s (solution A). On parallel, TiO_2 powder was also dispersed in ethanol and sonicated for 60 s (solution B). Afterwards, the mixture of solution A and B was sonicated for 60 s followed by mixing with a magnetic stirrer for 12 h. Then, the nanocomposites were separated by a permanent magnet, washed with the same procedure as the MCNT synthesis (i.e. using ethanol followed by ultrapure water) and dried at 105 °C overnight. Five different MCNT- TiO_2 nanocomposites were prepared with the mass ratio of MCNT over TiO_2 of 10:1, 5:1, 1:1, 1:5 and 1:10. These mass ratios were selected based on our previous evaluation, where the optimum mass ratio between MCNT over TiO_2 was within this range (Awfa et al., 2019).

2.3. Characterization of MCNT- TiO_2 nanocomposites

The carbon contents in the MCNT and the five MCNT- TiO_2 nanocomposites were determined using gravimetry method by calcining the samples at 700 °C for 2 h (Yap and Lim, 2012). The

crystallinity of MCNT and MCNT-TiO₂ were determined with X-ray diffraction (XRD) in Rigaku MiniFlex 600 powder diffraction meter using Cu K α ($\lambda = 1.5406 \text{ \AA}$) radiation and recording 2θ range from 10 to 80°. Brunauer-Emmet-Teller (BET) method by nitrogen adsorption at 77 K obtained with Micromeritics ASAP 2020, Japan, determined the specific surface area and the pore volumes. Transmission electron microscopy-energy dispersive X-ray spectroscopy (TEM-EDX) was used to observed samples microstructure and elements (JEM-2010F). Fourier transform infrared (FT-IR) spectrometer (JASCO FTIR 4600, Japan) was used to measure FT-IR spectra of the samples in the range of 4000–400 cm⁻¹ using KBr plate. Samples morphologies were analyzed with a scanning electron microscopy (SEM) operating (Hitachi SU9000, Japan). Magnetic properties of the samples were measured by using a vibrating sample magnetometer (VSM). All of the magnetization results were normalized with the total weight of the sample.

2.4. Incubation and counting of *E. coli*

Fresh liquid cultures of *E. coli* were prepared by inoculation in an LB nutrient medium and incubation at 37 °C for 24 h under constant stirring on a shaker (stationary phase). To prepare the reaction suspensions, 1.0 mL of the liquid culture was centrifuged at 3000 rpm for 15 min at 4 °C to recover the bacteria and washed with phosphate buffer two times. Prepared *E. coli* suspension was diluted to achieve an initial concentration of bacteria (1.0–2.0 × 10⁶ CFU mL⁻¹). For the bacteria counting, plate dilution method was employed. Briefly, the sample solution was diluted with proper rate using sterilized ultrapure water and mixed with LB agar medium. Three plates were prepared for each dilution rate. After incubation for 24 h at 37 °C, the emerged colonies were counted.

2.5. Photocatalytic disinfection experiment

Specific concentrations of bacterial strains (1.0–2.0 × 10⁶ CFU mL⁻¹, 100 mL) were mixed with appropriate load of catalyst (0.10, 0.25, 0.50 and 1.00 g L⁻¹) and mass ratio between MCNT and TiO₂ (10:1, 5:1, 1:1, 1:5 and 1:10). The variation in the load of catalysts were chosen based on the previous photocatalytic disinfection studies (Rincón and Pulgarin, 2003). However, optimum catalyst loading might be different from each study and it should be noted that high loading of the catalyst can lead to increasing the treatment cost. Bare MCNT and TiO₂ were also tested. A solar simulator (MS-35AAA, Ushio Lighting Edge Technologies, Japan) at maximum wavelength of 550 nm with an intensity of 1000 W m⁻² (i.e. 360 J cm⁻² for 60 min irradiation) was used as a light source and both presence and absence of the light were checked. The solution was mixed by a stirrer and the treated samples were collected at various contact time (0, 10, 20, 30 and 60 min). For the catalyst separation after the photocatalysis, a

permanent magnet was put under the beaker with the sample immediately after the contact time. The supernatant was taken after 5 min for the separation. Then, survived bacteria were counted by plate dilution method. For the bare TiO₂ case, the catalyst was not separated after the contact time because of no magnetic property and the solution containing TiO₂ was directly incubated for the bacterial enumeration. Because the previous studies reported that the SEM/TEM images and visual inspection of the Petri dish pictures did not demonstrate any evidence of TiO₂ effect on the plate count assays, it is assumed in this study that the results are comparable to the sample with MCNT-TiO₂ separation (Uyguner-Demirel et al., 2018). After the disinfection, MCNT-TiO₂ was observed by SEM (FE-SEM S-4700 (HITACHI)) to confirm the structural changes of *E. coli* cells. All the experiment was run at room temperature. The pH was maintained at 7.0 using phosphate buffer solution. All the glassware was autoclaved at 120 °C for 15 min before use. Duplications were prepared for each sample. First order equation (Eq. (1)) was employed to evaluate the kinetics.

$$\ln \frac{N}{N_0} = -kt \quad (1)$$

where N is viable population of bacteria at time t , N_0 is initial bacteria population, and k is reaction rate constant.

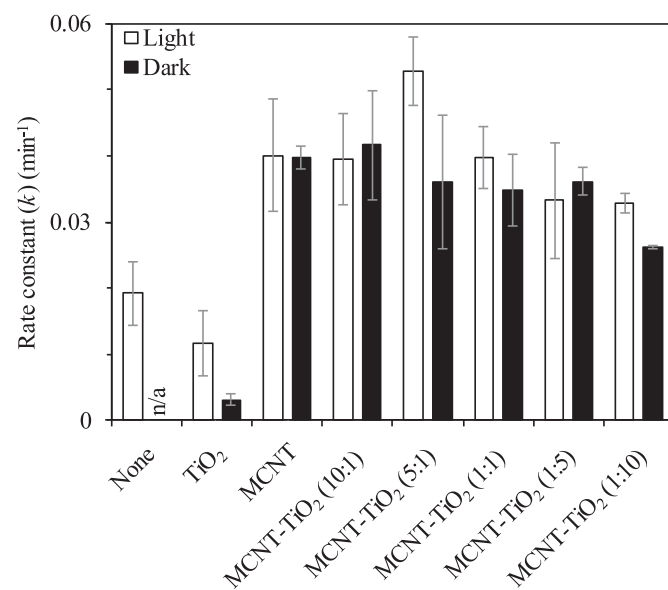


Fig. 1. First order rate constants of *E. coli* disinfection from the disinfection experiment using MCNT-TiO₂ with different MCNT ratio (R^2 : 0.81–0.99). Catalyst concentration was 0.50 g L⁻¹. Error bars represent \pm (standard deviation) from duplicate experiments where cell counting was conducted in triplicate.

Table 1
Characteristics of TiO₂, MCNT, and MCNT-TiO₂ nanocomposites used in this study.

Catalysts	Carbon Contents (%)	SA (m ² g ⁻¹)	PV _{total} (cm ³ g ⁻¹) [%]	PV _{micro} (cm ³ g ⁻¹) [%]	PV _{meso} (cm ³ g ⁻¹) [%]	PV _{macro} (cm ³ g ⁻¹) [%]	Magnetization (emu g ⁻¹)
TiO ₂	–	56	0.24 [100]	0.002 [0.8]	0.13 [53.7]	0.11 [45.5]	–
MCNT	94	201	1.50 [100]	0.01 [0.7]	0.75 [50]	0.74 [49.3]	0.68
MCNT-TiO ₂ (10:1)	87	188	1.92 [100]	0.01 [0.5]	1.11 [57.9]	0.80 [41.6]	0.45
MCNT-TiO ₂ (5:1)	71	177	1.44 [100]	0.01 [0.7]	0.76 [52.9]	0.67 [46.4]	0.44
MCNT-TiO ₂ (1:1)	51	156	1.26 [100]	0.01 [0.8]	0.66 [52.1]	0.59 [47.1]	0.41
MCNT-TiO ₂ (1:5)	32	151	1.20 [100]	0.01 [0.8]	0.65 [54.4]	0.54 [44.8]	0.34
MCNT-TiO ₂ (1:10)	28	144	1.18 [100]	0.01 [0.8]	0.61 [52]	0.56 [47.2]	0.33

SSA is specific surface area, PV_{total} is total pore volume, PV_{micro} is the volume of micropores (i.e., PV < 2 nm), PV_{meso} is the volume of mesopores (i.e., 2 < PV < 50 nm), and PV_{macro} is the volume of macropores (i.e., PV > 50 nm).

To reveal the effect of each ROS, scavenger studies were also conducted. Isopropanol and sodium oxalate were used as scavengers for $\cdot\text{OH}$ and valence band holes (h^+), respectively (Cruz-Ortiz et al., 2017).

One-way analysis of variance (ANOVA) and post hoc comparison using Tukey's Honestly Significant Difference Test (Tukey's HSD) were applied to compare the first order rate constant (k) for different catalysts, catalyst concentrations and ROS scavengers. Student t -test was conducted to compare the difference of k under light and dark conditions.

2.6. Kinetic model application

The traditional empirical kinetic models for photocatalytic disinfection (i.e. Chick (Eq. (1)), Chick-Watson (Eq. (2)), Hom (Eq. (3)) and modified Hom (Eq. (4)) were applied to fit the experimental results.

$$\ln \frac{N}{N_0} = -kC^n t \quad (2)$$

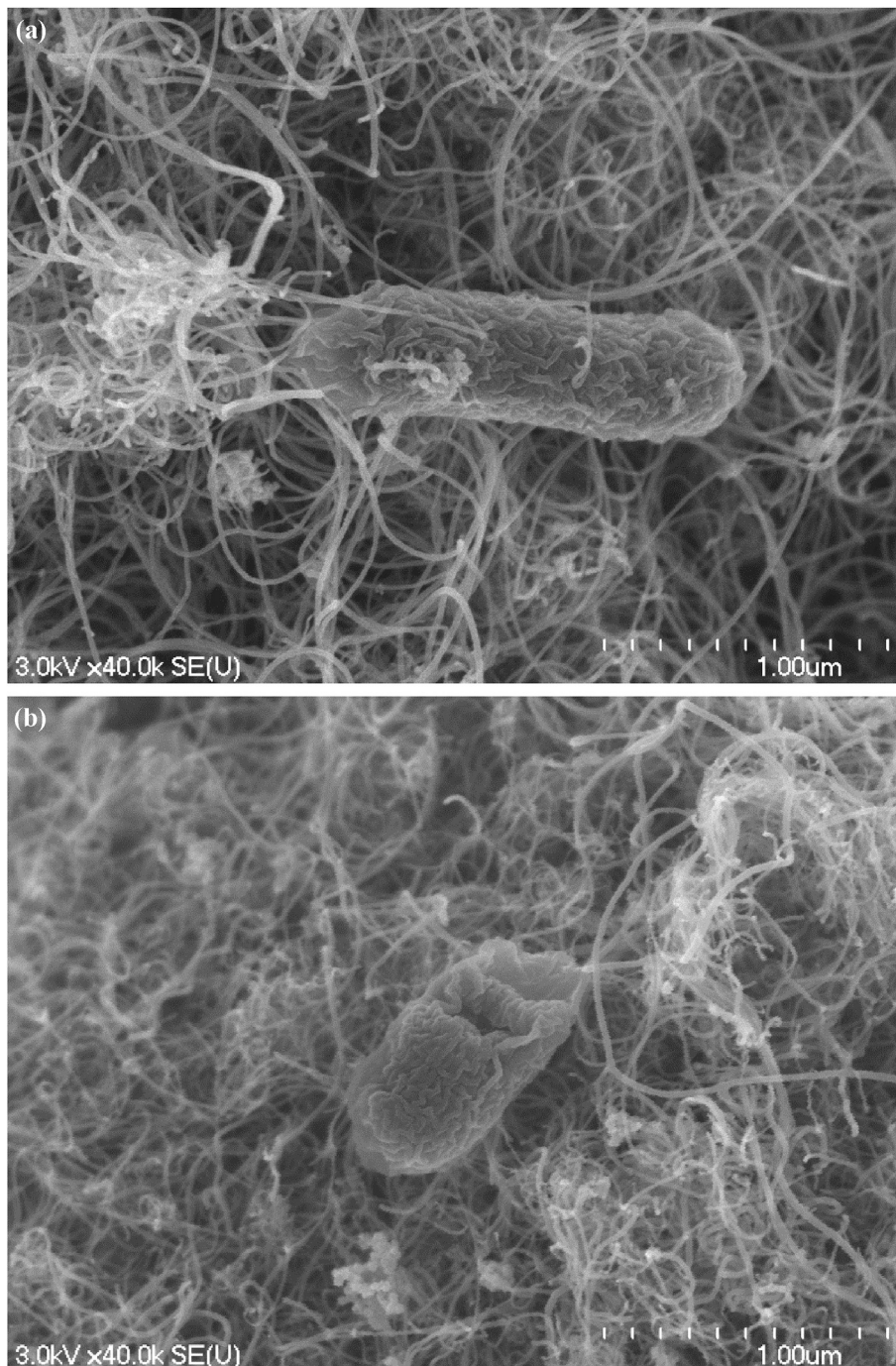


Fig. 2. SEM images of *E. coli* on MCNT-TiO₂ in case (a) without light and (b) with light. Catalyst concentration was 1.0 g L⁻¹. The mass ratio of MCNT over TiO₂ was 5:1.

$$\ln \frac{N}{N_0} = -kC^n t^m \quad (3)$$

$$\ln \frac{N}{N_0} = -k_1 [1 - \exp(-k_2 t)]^{k_3} \quad (4)$$

where N is the viable population of bacteria at time t , N_0 is the initial microbial population, k is the reaction rate constant, C is the concentration of the disinfectant, and m and n are the empirical constants.

As a more mechanistic model, Langmuir-Hinshelwood (LH) based kinetic model (Eq. (5)) was also applied to the results (Marugán et al., 2008). Because MCNT-TiO₂ can act as a good adsorbent, the assumption for the photocatalytic disinfection kinetic model based on adsorption approach (i.e. LH model) is expected to be reasonable. Plus, the constants derived from this model have physical meanings while those from the traditional empirical models sometimes do not. Thus the LH based model enhances more the understanding of the mechanism.

$$\frac{dN}{dt} = \frac{kKN^n}{1 + KN^n} \quad (5)$$

where N is the viable population of bacteria at time t , k is the rate constant of the reaction of ROS with bacteria, K represents pseudo-adsorption constant, and n is the inhibition coefficient coming from the competition for ROS between bacteria and intermediate compounds. Nonlinear regression by Microsoft excel solver was used to find the constants.

3. Results and discussion

3.1. Materials characterization

The characteristics of the materials used in this study (i.e. carbon contents, specific surface area (SSA), pore volume distribution and magnetization) are shown in Table 1. The magnetization and SSA decreased with the increment of TiO₂ mass, which confirm the anchorage of TiO₂ on the surface of MCNT (Fig. S1 and Table 1). Due to non-homogeneous distribution of magnetic nanoparticle inside the CNT, the magnetization for different MCNT-TiO₂ mass ratios are not proportionally linear with the amount of MCNT (Ateia et al., 2017). PV distribution showed that meso pores (i.e. PV = 2–50 nm) and macro pores (i.e. PV > 50 nm) were dominant for all samples. SEM images of bare TiO₂, MCNT and nanocomposite with different mass ratios of MCNT over TiO₂ are shown in Fig. S2. The surface of MCNT-TiO₂ was covered by TiO₂ aggregates at lower MCNT ratio over TiO₂. TEM images and EDX analysis indicated that cobalt particles were in the tubes and they were the major source of the magnetic property of MCNT (Fig. S3 and Fig. S4). These metallic cobalt particles accounted for ~6% of the nanocomposite mass content (Table 1). Previous studies also reported that the metallic content (i.e. Fe, Ni, or Co) led to the inherent magnetic characteristics of MCNT (Vejpravova et al., 2016). The presence of cobalt inside MCNT-TiO₂ system will not affected the photocatalytic disinfection mechanism of MCNT-TiO₂, because these metallic particles are stable and difficult to release, even in concentrated acids at high temperature (Ateia et al., 2017).

The surface chemistry of the samples was characterized by FT-IR (Fig. S5). For both of MCNT-TiO₂ nanocomposites and pristine TiO₂, a peak at 450 cm⁻¹ was observed, which is assigned to Ti–O bond. Peaks at 3730 cm⁻¹ and 3380 cm⁻¹ were assigned to O–H stretching. Other peaks were observed at 1520 cm⁻¹ and 970 cm⁻¹ indicated C=C bond. In addition, peaks at 690 cm⁻¹ were

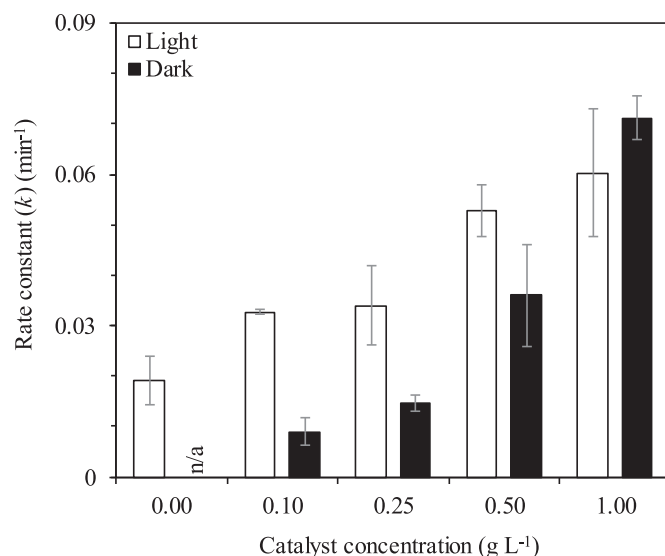


Fig. 3. First order rate constants of *E. coli* disinfection from the disinfection experiment using MCNT-TiO₂ with different catalyst concentrations (R^2 : 0.83–0.97). The mass ratio of MCNT over TiO₂ was 5:1. Error bars represent \pm (standard deviation) from duplicate experiments where cell counting was conducted in triplicate.

induced by the frequency of C–H (Wang and Zhou, 2010). Two main XRD diffraction peaks were observed in MCNT ($2\theta = -26^\circ$ and 43°) due to its graphene like structure (Fig. S6) (Ateia et al., 2017). Two peaks in bare TiO₂ consisted of both anatase ($2\theta = -25.3^\circ$) and rutile ($2\theta = -27.4^\circ$) TiO₂, and all MCNT-TiO₂ nanocomposites showed these two peaks that were consistent with the mass ratio of MCNT and TiO₂. In case of low TiO₂ content, an overlap with MCNT peaks was observed. The diffraction peak of TiO₂ contained both anatase (main diffraction peak at $2\theta = -25.3^\circ$) and rutile (main diffraction peak at $2\theta = -27.4^\circ$) TiO₂ peaks. Ye et al. (2018) reported that the polymorphous of TiO₂ (i.e. a mixture of anatase and rutile) have shown better photocatalytic activity and narrower band gap than each of them individually.

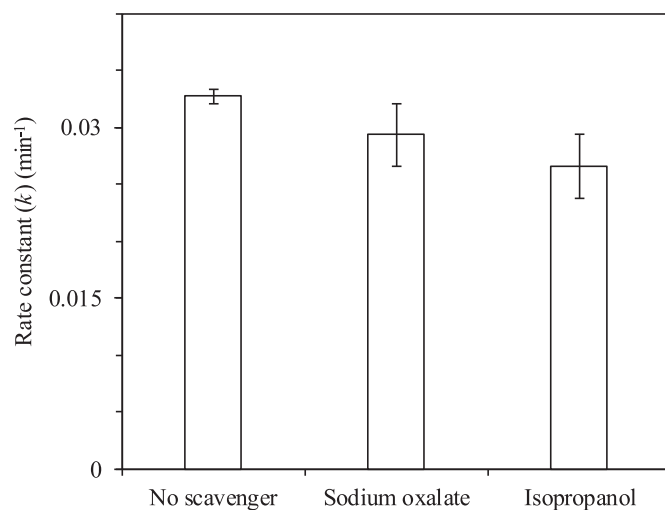


Fig. 4. First order rate constants of *E. coli* disinfection from the disinfection experiment using different scavengers (R^2 : 0.97–0.98). The mass ratio of MCNT over TiO₂ was 5:1. Catalyst concentration was 0.10 g L⁻¹. Error bars represent \pm (standard deviation) from duplicate experiments where cell counting was conducted in triplicate.

3.2. Effect of MCNT:TiO₂ mass ratio on the disinfection activity

Photocatalytic disinfection experiments using the catalysts with different MCNT:TiO₂ mass ratio were conducted on the assumption that both photocatalytic and physical inactivation or removal occurred under the light condition, but only physical inactivation/removal happened under the dark condition (Kang et al., 2008; Koli et al., 2016b; Moon and Kim, 2010). As shown in Fig. 1, under light, the overall reaction rate constants of MCNT-TiO₂ were significantly higher than the bare TiO₂ and the direct photolysis (Turkey's HSD, $p < 0.05$). Higher photocatalytic disinfection of MCNT-TiO₂ can be attributed to the increment of reactive surface area, extension of wavelength absorption to the visible light region (i.e. band gap reduction), and suppression of electron-hole recombination (Koli et al., 2016b; Zhang and Oh, 2010). Under light, the rate constant of MCNT-TiO₂ mass ratio of 5:1 ($k = 0.52 \pm 0.005 \text{ min}^{-1}$) was statistically significantly higher than MCNT-TiO₂, bare TiO₂ and MCNT (Tukey's HSD, $p < 0.05$) (Fig. 1). Apparently, excess MCNT weakens the photocatalytic ability due to the lack of TiO₂, and decreasing the MCNT content limits the physical capture and interaction between MCNT and TiO₂ due to the aggregation of TiO₂ (Akasaka and Watari, 2009; Koli et al., 2016b). It should be highlighted that the reaction rates of bare TiO₂ were lower than direct photodisinfection (i.e. experiments without catalyst). The possible reasons for this reduction include the light scattering effect of by TiO₂ particles as well as the weak light penetration into the solution (Rincón and Pulgarin, 2003).

3.3. The role of MCNT and TiO₂ in the nanocomposite on the disinfection activity

For the optimum MCNT-TiO₂ ratio (i.e. 5:1), the difference between light and dark conditions was much larger (i.e. more than 45% increase) than the other cases (only < 25% increase), and was statistically significant (Student *t*-test, $p < 0.05$). The limited effect of light under the other conditions indicates that physical bacterial removal or inactivation by MCNT was more dominant than photocatalytic disinfection. In addition, SEM images revealed that light killed the captured bacteria on the surface of MCNT-TiO₂, while the morphology of *E. coli* under treatment without light retained the smooth surface on MCNT-TiO₂ (Fig. 2). This was possibly because of the high carbon content reduces the light adsorption and thus decrease the performance of TiO₂ to produce radical for photocatalytic disinfection (Moon and Kim, 2010). It should be noted that SEM images with single cell may not be representative for all bacteria community (Sondi and Salopek-Sondi, 2004);

nevertheless, we saw similar observations in other SEM images under light and dark conditions (data not shown).

Interestingly, previous studies reported that CNT-TiO₂ with low carbon contents (i.e. 0.5 wt%) showed the best bactericidal disinfection (Koli et al., 2016a, 2016b). However, they did not separate the catalyst after the reaction and directly incubated the bacteria with the catalyst. Therefore, it is expected that they counted the captured bacteria as remained in water. In contrast, our experiment clearly distinguished the captured bacteria from free bacterial cells in water. Such different experimental approaches might result in the different optimum mass ratio between CNT and TiO₂. Nevertheless, SEM analysis found similar observations in the previous studies. Kang et al. (2008) reported the *E. coli* destruction by single-wall CNT but multi-wall CNT (i.e. same as this study) did not destroy the bacteria. In the case of the photocatalysis, Liu et al. (2019) showed the SEM images that revealed the *E. coli* inactivation.

3.4. Effect of MCNT-TiO₂ concentration on the disinfection activity

The highest rate constant (i.e. 0.06 min^{-1}) was recorded when MCNT-TiO₂ loading was 1.00 g L^{-1} (Fig. 3), significantly higher than the loading of 0.10 and 0.25 g L^{-1} (Tukey's HSD, $p < 0.05$) while not significantly higher than the case of 0.50 g L^{-1} (Tukey's HSD, $p > 0.05$). On the other hand, the difference in rate constants between light and dark condition (i.e. the effect of light) was the largest at the catalyst concentration of 0.10 g L^{-1} (Student *t*-test, $p < 0.001$), and it decreased with the increment of the catalyst concentration, indicating that 0.10 g L^{-1} was the best for the photocatalytic activity (i.e. 0.033 min^{-1}). It means that the light effect (i.e. photocatalytic reaction) decreased proportionally to the increment of the catalyst loading while physical removal/inactivation showed the opposite trend. This is probably because the turbidity caused by the high catalyst concentration attenuate light penetration to the active site of the catalyst (Maness et al., 1999) and at the same time the high catalyst concentration provide more active adsorption sites, resulting in the dominant physical removal (Akasaka and Watari, 2009).

3.5. Effect of different ROS species on the disinfection activity

When the photocatalyst is irradiated by light with a proper wavelength, h^+ are generated and it oxidize H₂O to produce $\cdot\text{OH}$. Then, the produced $\cdot\text{OH}$ as well as h^+ can disinfect bacteria due to their high oxidizability (Lebedev et al., 2018). The experiment highlighting the role of each ROS showed that the decrease in both total removal and rate constant was observed when either

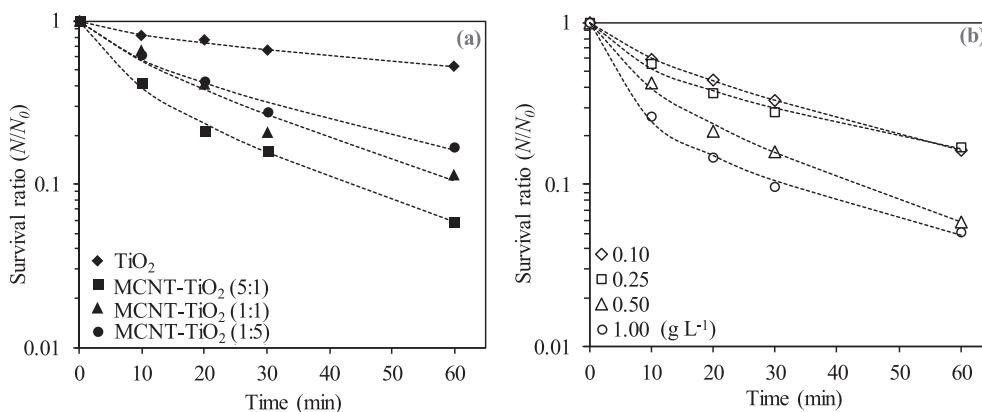


Fig. 5. *E. coli* survival ratio transition with time from the disinfection experiment using (a) different mass ratio of MCNT over TiO₂, and (b) different concentration of MCNT-TiO₂. Dotted lines show the curves obtained from Hom model.

scavenger was added, and isopropanol inhibited disinfection process more than sodium oxalate (Fig. 4). The significant decrease in rate constants when adding scavengers (Tukey's HSD, $p < 0.05$) proved that not only the physical interaction between bacteria and MCNT-TiO₂ but also the photocatalytic reaction indeed took place, and the inactivation due to •OH produced by photocatalyst was the dominant mechanism in the disinfection process. In a previous study, Ouyang et al. (2016) used C₇₀-TiO₂ hybrid as a photocatalyst for *E. coli* O157:H7 disinfection under visible light and also observed that •OH was more dominant than valence band (VB).

3.6. The role of each component in the nanocomposite in the disinfection process

Previous study indicated that disinfection model showed good prediction ($R^2 > 0.8$) for the physical removal of organic pollutant by carbon material (i.e. activated carbon) (Ziska et al., 2016). Therefore, the existing disinfection model could be useful to explain the role of each component in MCNT-TiO₂; where physical separation of *E. coli* can be a major removal role. Among the applied four models, modified Hom model showed the best fit to the results ($R^2 = 1.00$) (Fig. S7). This is because only modified Hom model can explain an initial delay due to the time required for the damage accumulation, a log-linear disinfection region and a final tail because of the presence of a microbial subpopulation resistant to the disinfection simultaneously (Chong et al., 2010; Marugán et al., 2008). Hom model also showed a good R^2 value (i.e. 0.99), which was similar to modified Hom model. On the other hand, Chick model ($R^2 = 0.90$) and Chick-Watson model ($R^2 = 0.90$) fitted relatively worse than the others. Because clear shoulder curves at the initial phase of the reaction were not observed in the results while there were obvious tailing offs at the end of the reaction (Fig. 5), the models that can explain the tailing off fitted well (i.e. Hom and modified Hom model). Although modified Hom model showed the best R^2 value among the four models, two of the three constants (i.e. k_1 and k_3) do not have physical meanings, and thus cannot infer the disinfection mechanisms. Herein, Hom model was employed as a next step to discuss the linkage of its rate constant to the experimental parameters.

As the result of the application of Hom model, Fig. 6 explains the relationships between the rate constant k and experimental parameters (i.e. carbon contents, SSA and catalyst concentration) (Table 1), and all the parameters showed the linear relationships with k value for MCNT-TiO₂. Positive correlation between carbon contents and k indicates the dominant effect of physical interaction of bacteria with the catalyst, and this explanation does not contradict with the experimental results. The k values obtained from TiO₂ were out of the correlation and almost same as the smallest one among the MCNT-TiO₂ cases.

LH based kinetic model also fitted well to the results (i.e. R^2 was 0.99, Fig. S8), and there were clear relationships between two constants (i.e. k and K), and carbon contents, SSA and the catalyst concentration (Fig. 7). The value of k , the rate constant of the reaction of ROS with bacteria, drastically decreased between 28% and 32% of carbon contents, 144 m² g⁻¹ and 151 m² g⁻¹ of SSA, and 0.10 g L⁻¹ and 0.25 g L⁻¹ of the catalyst concentration. At the same point, the value of K , pseudo-adsorption constant, jumped up. This result is because high carbon contents, that led to higher SSA, and high concentration of the catalyst allowed more adsorption and limited the interaction with ROS (i.e. photocatalysis). In addition, it inferred that the dominant bacterial removal/inactivation mechanism shifted from the photocatalysis to the physical reaction at certain points in terms of the tested parameters (i.e. carbon contents, SSA and catalyst concentrations). For the values of n , there were no correlations with the experimental parameters (data not

shown), and therefore, it is concluded that the effect of the reaction inhibition due to the competition for ROS between bacteria and intermediate compounds was not controlled by these experimental parameters.

4. Conclusions

In this study, the deactivation mechanism of *E. coli* using MCNT-TiO₂ nanocomposites was investigated under solar light irradiation.

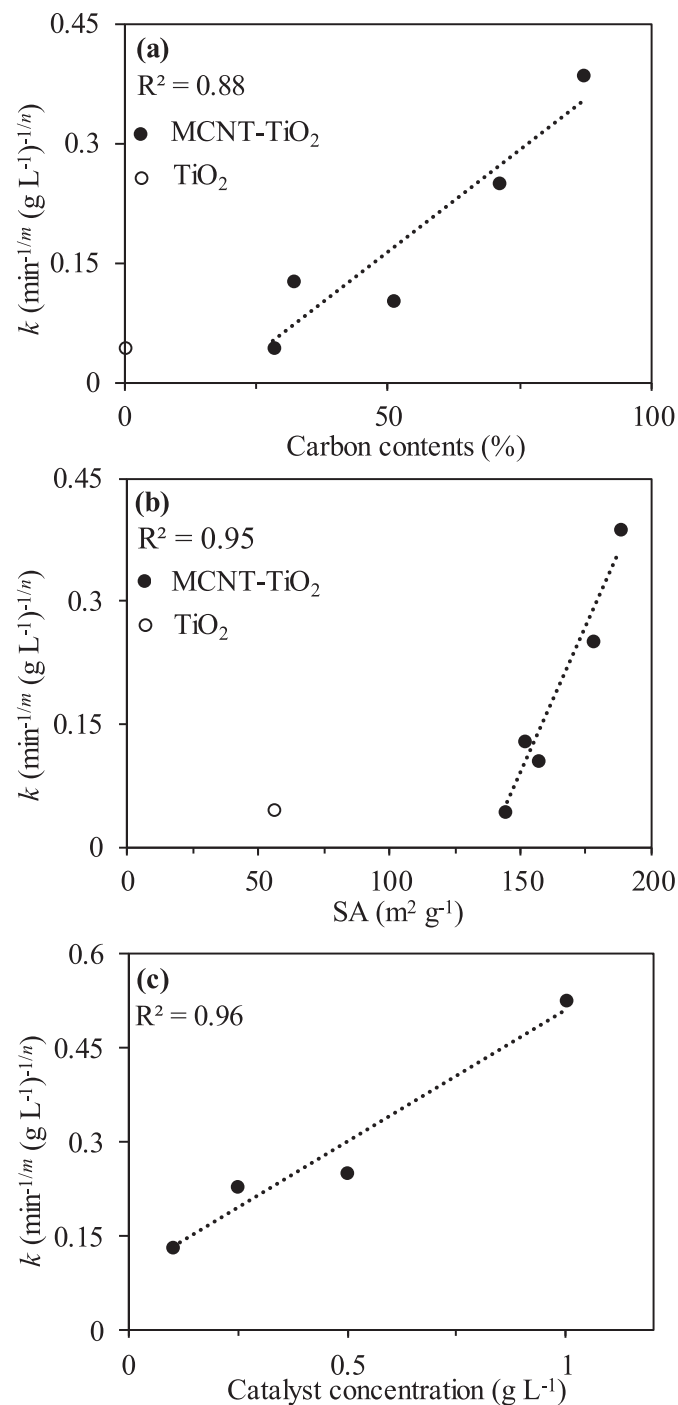


Fig. 6. Influence of (a) carbon contents (catalyst concentration: 0.50 g L⁻¹), (b) SSA (catalyst concentration: 0.50 g L⁻¹) and (c) the catalyst concentration (catalyst type: MCNT-TiO₂ (5:1)) on k from Hom model. Approximately straight lines for MCNT-TiO₂ plots were shown as dotted lines.

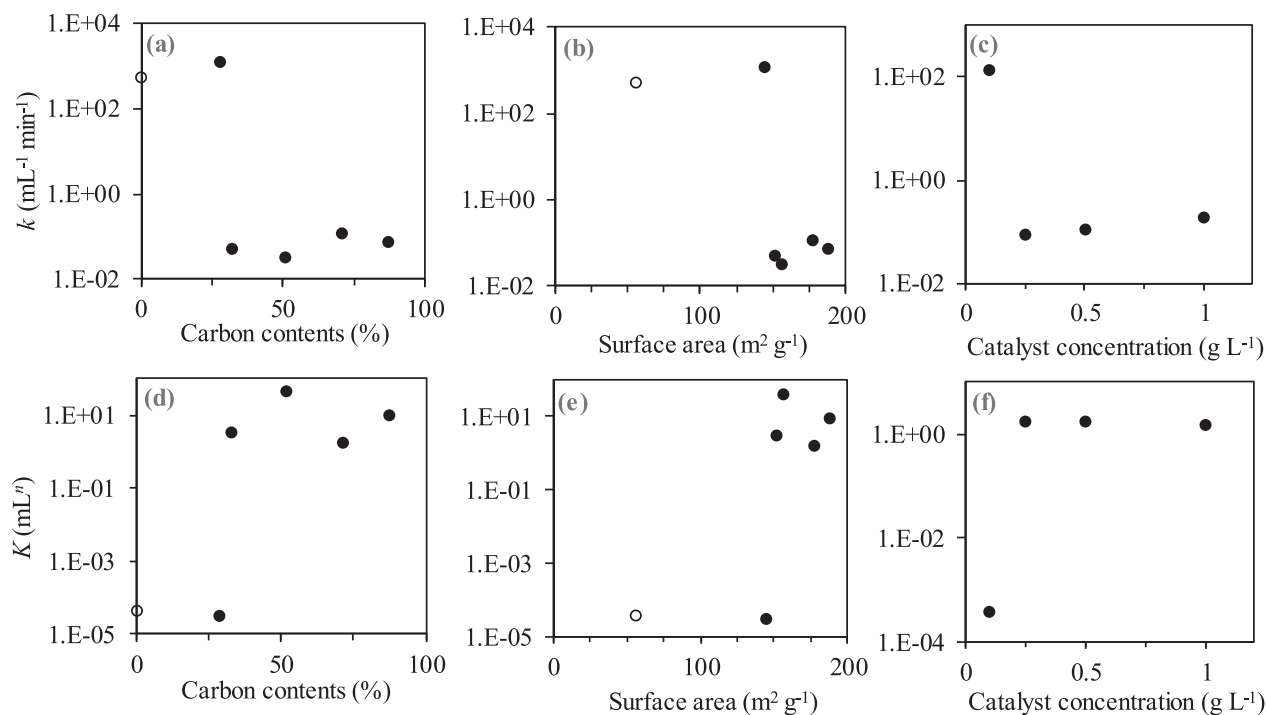


Fig. 7. Influence of (a) carbon contents on k , (b) SSA on k (catalyst concentration: 0.50 g L^{-1}), (c) catalyst concentration on k , (d) carbon contents on K (catalyst concentration: 0.50 g L^{-1}), (e) SSA on K , and (f) catalyst concentration on K (catalyst type: MCNT-TiO₂ (5:1)). Solid circles (●) and open circles (○) were MCNT-TiO₂ and TiO₂, respectively. k and K were obtained from LH based model.

The main findings and recommendations for future studies are summarized as follows:

- The optimum ratio of MCNT over TiO₂ and catalyst concentration for the experimental condition in this study were 5:1 and 1.0 g L^{-1} , respectively. However, in terms of the photocatalytic reaction, the best concentration was 0.10 g L^{-1} , and •OH worked as the dominant ROS.
- The physical bacterial capture and/or inactivation happened at the same time with the photocatalytic process, and it contributed dominantly to the overall bacterial removal especially when the catalyst concentration was high.
- Photocatalytic oxidation could kill the captured bacteria by MCNT-TiO₂ and remaining damaged cells were observed within the bundles of nanotubes.
- Carbon contents, SSA and concentration of MCNT-TiO₂ are likely related to the contribution rate of physical and photocatalytic reaction, and the dominant bacterial removal/inactivation mechanism shifted from photocatalysis to physical reaction as the dose of the nanocomposite increased.

For the further work, the following points are recommended.

- For deeper understanding of the disinfection mechanisms and the mechanistic model applicability, the relationships between rate constant (k) and other experimental parameters (e.g. light intensity and initial bacterial concentrations) need to be investigated.
- Since the contribution rate of physical and photocatalytic reaction to the whole disinfection process can be controlled, disinfection by MCNT-TiO₂ is a simple and fast removal process of bacteria (i.e., physical) and is continuous bacterial inactivation process (i.e. photocatalysis).

- More studies should address the optimization and the application of CNT-TiO₂ for water disinfection under realistic conditions (e.g. in the presence of natural organic matter and turbidity), which might be influential on the system performance.

Acknowledgments

Analyses of SEM, TEM, EDX, and XRD were supported by Ookayama Materials Analysis Division Technical Department in Tokyo Institute of Technology, and this work was supported by JSPS KAKENHI (Grant Number 18H01566). In addition, the authors would like to acknowledge Dr Manabu Fujii for his supportive discussion and Dr. Ji Shi and Dr. Takashi Harumoto for vibrating sample magnetometer analyses. Dion Awfa is grateful for a scholarship from Indonesia Endowment Fund for Education (LPDP).

Appendix A. Supplementary data

Supplementary data to this article can be found online at <https://doi.org/10.1016/j.chemosphere.2019.07.006>.

References

- Akasaka, T., Watari, F., 2009. Capture of bacteria by flexible carbon nanotubes. *Acta Biomater.* 5, 607–612. <https://doi.org/10.1016/j.actbio.2008.08.014>.
- Ateia, M., Ceccato, M., Budi, A., Ataman, E., Yoshimura, C., Johnson, M.S., 2018. Ozone-assisted regeneration of magnetic carbon nanotubes for removing organic water pollutants. *Chem. Eng. J.* <https://doi.org/10.1016/j.cej.2017.10.166>.
- Ateia, M., Erdem, C.U., Ersan, M.S., Ceccato, M., Karanfil, T., 2019. Selective removal of bromide and iodide from natural waters using a novel AgCl-SPAC composite at environmentally relevant conditions. *Water Res.* 156, 168–178. <https://doi.org/10.1016/j.watres.2019.03.028>.
- Ateia, M., Koch, C., Jelavic, S., Hirt, A., Quinson, J., Yoshimura, C., Johnson, M., 2017. Green and facile approach for enhancing the inherent magnetic properties of carbon nanotubes for water treatment applications. *PLoS One* 12, 1–21. <https://doi.org/10.1371/journal.pone.0180636>.
- Awfa, D., Ateia, M., Fujii, M., Johnson, M.S., Yoshimura, C., 2018. Photodegradation of

- pharmaceuticals and personal care products in water treatment using carbonaceous-TiO₂ composites: a critical review of recent literature. *Water Res.* 142, 26–45. <https://doi.org/10.1016/j.watres.2018.05.036>.
- Awfa, D., Ateia, M., Fujii, M., Yoshimura, C., 2019. Novel magnetic carbon nanotube-TiO₂ composites for solar light photocatalytic degradation of pharmaceuticals in the presence of natural organic matter. *J. Water Process Eng.* 31, 100836. <https://doi.org/10.1016/j.jwpe.2019.100836>.
- Ayekoe, C.Y.P., Robert, D., Lanciné, D.G., 2017. Combination of coagulation-flocculation and heterogeneous photocatalysis for improving the removal of humic substances in real treated water from Agbó River (Ivory-Coast). *Catal. Today* 281, 2–13. <https://doi.org/10.1016/j.cattod.2016.09.024>.
- Bennett, A., 2008. Drinking water: pathogen removal from water - technologies and techniques. *Filtr. Sep.* 45, 14–16. [https://doi.org/10.1016/S0015-1882\(08\)70495-6](https://doi.org/10.1016/S0015-1882(08)70495-6).
- Brookman, Ryan M., Lamsal, R., Gagnon, G.A., 2011. Comparing the formation of bromate and bromoform due to ozonation and UV-TiO₂ oxidation in seawater. *J. Adv. Oxid. Technol.* 14, 23–30. <https://doi.org/10.1515/jaots-2011-0103>.
- Chong, M.N., Jin, B., Chow, C.W.K., Saint, C., 2010. Recent developments in photocatalytic water treatment technology: a review. *Water Res.* 44, 2997–3027. <https://doi.org/10.1016/j.watres.2010.02.039>.
- Cruz-Ortiz, B.R., Hamilton, J.W.J., Pablos, C., Díaz-Jiménez, L., Cortés-Hernández, D.A., Sharma, P.K., Castro-Alfárez, M., Fernández-Ibañez, P., Dunlop, P.S.M., Byrne, J.A., 2017. Mechanism of photocatalytic disinfection using titania-graphene composites under UV and visible irradiation. *Chem. Eng. J.* 316, 179–186. <https://doi.org/10.1016/j.cej.2017.01.094>.
- Friedmann, D., Mendive, C., Bahemann, D., 2010. TiO₂ for water treatment: parameters affecting the kinetics and mechanisms of photocatalysis. *Appl. Catal. B Environ.* 99, 398–406. <https://doi.org/10.1016/j.apcatb.2010.05.014>.
- Ganguly, P., Byrne, C., Breen, A., Pillai, S.C., 2018. Antimicrobial activity of photocatalysts: fundamentals, mechanisms, kinetics and recent advances. *Appl. Catal. B Environ.* 225, 51–75. <https://doi.org/10.1016/j.apcatb.2017.11.018>.
- Kang, S., Herzberg, M., Rodrigues, D.F., Elimelech, M., 2008. Antibacterial effects of carbon nanotubes: size does matter! *Langmuir* 24, 6409–6413. <https://doi.org/10.1021/la800951v>.
- Kang, S., Pinaut, M., Pfefferle, L.D., Elimelech, M., 2007. Single-walled carbon nanotubes exhibit strong antimicrobial activity. *Langmuir* 23, 8670–8673. <https://doi.org/10.1021/la701067r>.
- King, C.H., Shotts, E.B., Wooley, R.E., Porter, K.G., 1988. Survival of coliforms and bacterial pathogens within protozoa during chlorination. *Appl. Environ. Microbiol.* 54, 3023–3033.
- Koli, V.B., Delekar, S.D., Pawar, S.H., 2016a. Photoinactivation of bacteria by using Fe-doped TiO₂-MWCNTs nanocomposites. *J. Mater. Sci. Mater. Med.* 27, 177. <https://doi.org/10.1007/s10856-016-5788-0>.
- Koli, V.B., Dhodamani, A.G., Raut, A.V., Thorat, N.D., Pawar, S.H., Delekar, S.D., 2016b. Visible light photo-induced antibacterial activity of TiO₂-MWCNTs nanocomposites with varying the contents of MWCNTs. *J. Photochem. Photobiol. A Chem.* 328, 50–58. <https://doi.org/10.1016/j.jphotochem.2016.05.016>.
- Krishna, V., Pumphreg, S., Lee, S.H., Zhao, J., Sigmund, W., Koopman, B., Moudgil, B.M., 2005. Photocatalytic disinfection with titanium dioxide coated multi-wall carbon nanotubes. *Process Saf. Environ. Protect.* 83, 393–397. <https://doi.org/10.1205/psep.04387>.
- Lebedev, A., Anariba, F., Tan, J.C., Li, X., Wu, P., 2018. A review of physicochemical and photocatalytic properties of metal oxides against *Escherichia coli*. *J. Photochem. Photobiol. A Chem.* 360, 306–315. <https://doi.org/10.1016/j.jphotochem.2018.04.013>.
- Li, Q., Mahendra, S., Lyon, D.Y., Brunet, L., Liga, M.V., Li, D., Alvarez, P.J.J., 2008. Antimicrobial nanomaterials for water disinfection and microbial control: potential applications and implications. *Water Res.* 42, 4591–4602. <https://doi.org/10.1016/j.watres.2008.08.015>.
- Li, Y., Yang, M., Zhang, X., Jiang, J., Liu, J., Yau, C.F., Graham, N.J.D., Li, X., 2017a. Two-step chlorination: a new approach to disinfection of a primary sewage effluent. *Water Res.* 108, 339–347. <https://doi.org/10.1016/j.watres.2016.11.019>.
- Li, Y., Zhang, X., Yang, M., Liu, J., Li, W., Graham, N.J.D., Li, X., Yang, B., 2017b. Three-step effluent chlorination increases disinfection efficiency and reduces DBP formation and toxicity. *Chemosphere* 168, 1302–1308. <https://doi.org/10.1016/j.chemosphere.2016.11.137>.
- Liu, N., Zhu, Q., Zhang, N., Zhang, C., Kawazoe, N., Chen, G., Negishi, N., Yang, Y., 2019. Superior disinfection effect of *Escherichia coli* by hydrothermal synthesized TiO₂-based composite photocatalyst under LED irradiation: Influence of environmental factors and disinfection mechanism. *Environ. Pollut.* 247, 847–856. <https://doi.org/10.1016/j.envpol.2019.01.082>.
- Maness, P.-C., Smolinski, S., Blake, D.M., Huang, Z., Wolfmum, E.J., Jacoby, W.A., 1999. Bactericidal activity of photocatalytic TiO₂ reaction: toward an understanding of its killing mechanism. *Appl. Environ. Microbiol.* 65, 4094–4098.
- Marugán, J., van Grieken, R., Sordo, C., Cruz, C., 2008. Kinetics of the photocatalytic disinfection of *Escherichia coli* suspensions. *Appl. Catal. B Environ.* 82, 27–36. <https://doi.org/10.1016/j.apcatb.2008.01.002>.
- Moon, H.M., Kim, J.W., 2010. Carbon nanotube clusters as universal bacterial adsorbents and magnetic separation agents. *Biotechnol. Prog.* 26, 179–185. <https://doi.org/10.1002/btpr.294>.
- Nieuwenhuijsen, M.J., Toledano, M.B., Eaton, N.E., Fawell, J., Toledano, B., Eaton, E., Elliott, P., Nieuwenhuijsen, J., 2000. Chlorination disinfection byproducts in water and their association with adverse reproductive outcomes: a review. *Occup. Environ. Med.* 57, 73–85. <https://doi.org/10.1136/oem.57.2.73>.
- Ouyang, K., Dai, K., Walker, S.L., Huang, Q., Yin, X., Cai, P., 2016. Efficient photocatalytic disinfection of *Escherichia coli* O157:H7 using C70-TiO₂ hybrid under visible light irradiation. *Sci. Rep.* 6, 25702. <https://doi.org/10.1038/srep25702>.
- Rincón, A., Pulgarin, C., 2003. Photocatalytic inactivation of *E. coli*: effect of (continuous–intermittent) light intensity and of (suspended–fixed) TiO₂ concentration. *Appl. Catal. B Environ.* 44 (3), 263–284.
- Sondi, I., Salopek-Sondi, B., 2004. Silver nanoparticles as antimicrobial agent: a case study on *E. coli* as a model for Gram-negative bacteria. *J. Colloid Interface Sci.* 275 (1), 177–182.
- Song, K., Mohseni, M., Taghipour, F., 2016. Application of ultraviolet light-emitting diodes (UV-LEDs) for water disinfection: a review. *Water Res.* 94, 341–349. <https://doi.org/10.1016/j.watres.2016.03.003>.
- Suárez-Iglesias, O., Collado, S., Oulego, P., Díaz, M., 2017. Graphene-family nanomaterials in wastewater treatment plants. *Chem. Eng. J.* 313, 121–135. <https://doi.org/10.1016/j.cej.2016.12.022>.
- Tarigh, G.D., Shemirani, F., Maz'hari, N.S., 2015. Fabrication of a reusable magnetic multi-walled carbon nanotube-TiO₂ nanocomposite by electrostatic adsorption: enhanced photodegradation of malachite green. *RSC Adv.* 5, 35070–35079. <https://doi.org/10.1039/c4ra15593a>.
- Thines, R.K., Mubarak, N.M., Nizamuddin, S., Sahu, J.N., Abdullah, E.C., Ganesan, P., 2017. Application potential of carbon nanomaterials in water and wastewater treatment: a review. *J. Taiwan Inst. Chem. Eng.* 72, 116–133. <https://doi.org/10.1016/j.jtice.2017.01.018>.
- Uyguner-Demirel, C.S., Birben, N.C., Bekbolet, M., 2018. A comprehensive review on the use of second generation TiO₂ photocatalysts: microorganism inactivation. *Chemosphere* 211, 420–448. <https://doi.org/10.1016/j.chemosphere.2018.07.121>.
- Vejpravova, J., Pacakova, B., Kalbac, M., 2016. Magnetic impurities in single-walled carbon nanotubes and graphene: a review. *Analyst* 141, 2639–2656. <https://doi.org/10.1039/c6an00248j>.
- Wang, S., Zhou, S., 2010. Photodegradation of methyl orange by photocatalyst of CNTs/P-TiO₂ under UV and visible-light irradiation. *J. Hazard Mater.* 185, 77–85. <https://doi.org/10.1016/j.jhazmat.2010.08.125>.
- Wilson, M.R., Jiang, Y., Villalta, P.W., Stornetta, A., Boudreau, P.D., Carrá, A., Brennan, C.A., Chun, E., Ngo, L., Samson, L.D., Engelward, B.P., Garrett, W.S., Balbo, S., Balskus, E.P., 2019. The human gut bacterial genotoxin colibactin alkylates DNA. *Science* (80-), Vol. 363. <https://doi.org/10.1126/science.aar7785>.
- Yap, P.-S., Lim, T.-T., 2012. Solar regeneration of powdered activated carbon impregnated with visible-light responsive photocatalyst: factors affecting performances and predictive model. *Water Res.* 46, 3054–3064. <https://doi.org/10.1016/j.watres.2012.03.008>.
- Ye, Y., Feng, Y., Bruning, H., Yntema, D., Rijnaarts, H.H.M., 2018. Photocatalytic degradation of metoprolol by TiO₂ nanotube arrays and UV-LED: effects of catalyst properties, operational parameters, commonly present water constituents, and photo-induced reactive species. *Appl. Catal. B Environ.* 220, 171–181. <https://doi.org/10.1016/j.apcatb.2017.08.040>.
- Zhang, F.-J., Oh, W.-C., 2010. Characterization and photonic effect of novel Ag-CNT/TiO₂ composites and their bactericidal activities. *Bull. Korean Chem. Soc.* 31, 1981–1987. <https://doi.org/10.5012/bkcs.2010.31.7.1981>.